Stem Cell Research & Therapy

RESEARCH

Open Access

Exploring the impact of gut microbiota-mediated regulation of exosomal miRNAs from bone marrow mesenchymal stem cells on the regulation of bone metabolism

Bin He[1,2†], Xianglin Shen[4†], Feng Li[3], Rudan Zhou[4], Haiyan Xue[4], Xianqiu Fan[4], Zhihua Wang[4], Xinpeng Guo[4], Yu Fan[4], Guanghu Luo[4], Xiujun Zhang[1,2*] and Hongyu Zheng[4*]

Abstract

Background Osteoporosis, which is a prevalent metabolic bone disease, is closely associated with imbalances in the gut microbiota.

Methods The ovaries of female 6-month-old Sprague–Dawley rats were surgically removed to induce osteoporosis. Subsequently, 16S rRNA sequencing was employed to characterize the gut microbiota in the osteoporotic rats. Bone marrow mesenchymal stem cells (BMSCs) were isolated from osteoporotic rats and cultured separately, and their osteogenic and adipogenic differentiation was observed. Furthermore, exosomes were extracted from these cells, and miRNA sequencing was performed on the exosomes to identify key miRNAs. Osteoporotic rats were then treated with a member of the gut microbiota, and changes in the osteogenic and adipogenic differentiation of BMSCs were observed.

Results In our investigation, we observed altered proportions of *Firmicutes* and *Bacteroidetes* in the guts of ovariectomized rats, which contributed to dysbiosis and subsequent changes in intestinal permeability. The BMSCs exhibited disrupted osteogenic/adipogenic differentiation, which was associated with structural damage to bones. Through the isolation of exosomes from BMSCs and subsequent miRNA analysis, we identified miR-151-3p and miR-23b-3p as potential pivotal regulators of bone metabolism. Furthermore, through 16S rRNA sequencing, we identified *g_Ruminococcus* and its marked capacity to ameliorate the imbalance in BMSC osteogenic/adipogenic differentiation. Intervention with *g_Ruminococcus* demonstrated promising outcomes, mitigating bone loss and structural damage to the tibia and femur in ovariectomized rats.

Conclusions These findings highlight the significant role of *g_Ruminococcus* in alleviating osteoporosis induced by estrogen deficiency, suggesting its therapeutic potential for addressing postmenopausal osteoporosis through the targeted modulation of BMSC-derived exosomal miR-151-3p and miR-23b-3p.

Keywords Ovariectomy, Osteoporosis, Gut microbiota, Exosomal miRNA, BMSC differentiation

†Bin He and Xianglin Shen have contributed to the work equally and should be regarded as co-first authors.

*Correspondence:
Xiujun Zhang
zhxj@ncst.edu.cn
Hongyu Zheng
zhenghongyu@kmmu.edu.cn
Full list of author information is available at the end of the article

Background

The gut microbiota plays crucial roles in various physiological processes, including bone metabolism, brain function, immune system regulation, liver metabolism, and respiratory health [1–5]. Alterations in genetically modified components and host responses can contribute to metabolic bone diseases [6]. For example, *Akkermansia muciniphila*, which is a mucin-adherent bacterium in the gut microbiota, exerts an anti-osteoporosis effect that manifests in bone tissue. This effect mitigates the osteoporotic phenotype induced by ovariectomy (OVX) by increasing osteogenic activity and decreasing osteoclast formation [7]. Moreover, the *Firmicutes* to *Bacteroidetes* ratio (F/B ratio) regulates mitochondrial biogenesis by modulating the key enzyme glutamate cysteine ligase catalytic subunit (Gclc). This regulation may be associated with metabolic diseases [8, 9], including postmenopausal osteoporosis [10]. Consequently, the gut microbiota can impact metabolic syndromes, such as osteoarthritis and osteoporosis [9]. Despite occasional contradictory data in the literature, studies have indicated that *Firmicutes* can modulate the expression of miRNAs that are associated with osteoporosis [11], suggesting their involvement in the development of osteoporosis. Researchers have reported that changes in miRNA expression can influence increased bone resorption and decreased bone density, contributing to the development of osteoporosis [12].

Mesenchymal stromal cells (MSCs) are a heterogeneous population found in most stromal tissues, comprising multipotent stem cells, progenitors, and differentiated cells [13, 14]. MSCs can differentiate into mesodermal derivatives, including osteocytes, chondrocytes, adipocytes, and muscle cells [15]. Their ability to differentiate into various mesenchymal tissues positions MSCs as promising candidates for treating bone and cartilage disorders. The bone formation process involving osteoblasts is orchestrated by bone marrow mesenchymal matrix/stem cells, which serve as progenitors for both osteoblasts and adipocytes [16]. These cells adhere to vascular endothelial cells, collectively forming the ecological niche of BMSCs [17]. Elevated levels of inflammatory factors, such as tumor necrosis factor-alpha (TNF-α) and interleukin-1 beta (IL-1β), can hinder the proliferation and function of BMSCs, impairing bone formation, causing decreases in bone mass and density, and promoting the accumulation of adipose tissue [18–20]. From a pharmacological perspective, targeted administration of interventions to BMSCs can restore their proliferation and osteogenic capabilities. Thus, directing interventions toward BMSCs has emerged as a viable strategy for stimulating osteoblast generation. Extracellular vehicles (EVs) are natural vesicles with optimal biocompatibility and stability. EVs can be genetically engineered for use as nanocarriers that target BMSCs through interactions with receptor ligands [21–23]. EVs are abundant in various bodily fluids, and they carry proteins, mRNAs, and miRNAs. Upon release, these EVs are taken up by neighboring or distant cells. EVs also contribute to the regulation of epigenetic processes through the transmission of miRNAs, influencing the biological functions of recipient cells in bone regeneration. Numerous studies have confirmed that BMSC-derived EVs can promote osteogenesis or inhibit osteoclast formation through miRNAs, ultimately increasing bone mass [24–27].

In this study, we investigated changes in the gut microbiota of ovariectomized rats, isolated exosomes from the BMSCs of OVX model rats, and screened differentially expressed miRNAs. Our aim was to explore the potential roles of distinct members of the gut microbiota as diagnostic and prognostic biomarkers of osteoporosis. A comparative analysis was performed on the exosomal miRNAs derived from BMSCs and the fecal microbiota of ovariectomized rats, aiming to elucidate the complex interactions among the gut microbiota, miRNAs, and osteoporosis. This integrative study of the gut microbiota and exosomal miRNAs from BMSCs will contribute to a deeper understanding of the mechanisms involved in the osteogenic and adipogenic differentiation of BMSCs. This, in turn, will aid in the identification of diagnostic biomarkers and potential therapeutic targets of postmenopausal osteoporosis, providing a relevant foundation for assessing the risk of osteoporosis.

Methods

Animals

For Experiment 1 (Fig. 1a), 20 female SD rats were purchased from Vital River Laboratories (Beijing, China). The rats were housed (5 rats per cage) in a standard specific pathogen-free (SPF) animal facility at Kunming Medical University. The barrier facility was maintained under conditions of temperature, humidity, and light–dark cycle of 22–26 °C, 40–60%, and 12/12 h, respectively. The rats were then randomly divided into the control ($n=10$) and OVX groups ($n=10$). All the animals were given free access to fresh water and food (Approval No. kmmu20210178).

For Experiment 2 (Fig. 1a), we randomly assigned 6-month-old female SD rats to three experimental groups, namely, the control group, the OVX group and the OVX with *Ruminococcus* transplantation group (*Ruminococcus* + OVX group) ($n=10$ in each group). This study was approved by the Ethics Committee of the First Affiliated Hospital of Kunming Medical University (Approval No. kmmu20210178). Random numbers were generated with the standard = RAND () function in

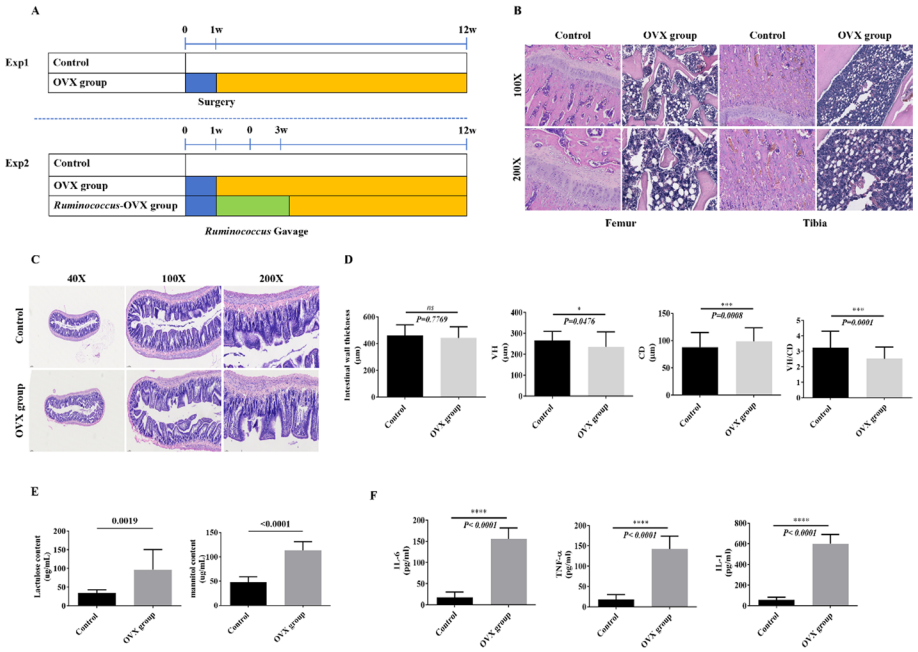

Fig. 1 Ovariectomy-induced osteoporosis in rats and its association with altered intestinal permeability. **a** Experimental design for ovarian removal surgery in female SD rats (Experiment 1) and experimental design for *Ruminococcus* intervention (Experiment 2). **b** Pathological changes in the femur and tibia observed at 100X (upper) and 200X (lower) magnification in the control and OVX groups. **c** Pathological changes in the ileum at 40X (left), 100X (middle), and 200X (right) magnifications in the control and OVX groups. **d** Measurements of the ileal wall thickness, villus height, crypt depth, and the ratio of villus height to crypt depth. The data are expressed as the means ± SDs. $n = 6$ per group. **e** Lactulose concentration in urine from the control and OVX groups. **f** Levels of peripheral blood IL-1, IL-6, and TNF-α in the control and OVX groups. The difference between the control and OVX groups was analyzed by Student's t test. The data are expressed as the means ± SDs. $n = 10$ per group (E, F). Exp, experiment; OVX, ovariectomized group; w, weeks

Microsoft Excel. The test time was between 08.30 am and 12.30 pm, and the testing order was randomized daily, and each animal was tested at a different time each test day.

After one week of acclimatization, bilateral oophorectomy was performed on the rats in the OVX group, following the protocol outlined in previous research [28]. Postsurgery, to prevent infection, intraperitoneal injections of penicillin were administered twice a day for two days. The control and OVX model rats received nonacidified sterilized water without antibiotics. The health of the rats was monitored by measuring their weight (weekly), food and water intake, and general animal activity, panting, and fur condition. All the recipient rats were anesthetized with a mixture of oxygen and isoflurane with a Matrx VMR small animal anesthesia machine (Fig. 1a). At the conclusion of the experiments, the rats were euthanized via CO_2 asphyxiation, following the guidelines set by the Ethics Committee of the First Affiliated Hospital of Kunming Medical University. After euthanasia, tissue samples were collected for analysis. This procedure was approved by the institutional animal ethics committee (Approval No. kmmu20210178, Approval Date: March 2, 2022), ensuring that all protocols complied with ethical standards for animal research. This study has been conducted in accordance with the ARRIVE guidelines 2.0 to ensure the transparency and reproducibility of animal research.

Histopathology

The left and right femurs and tibiae were fixed in 10% phosphate-buffered formalin at room temperature for 24 h. The samples were subsequently decalcified in 10% EDTA for 21 days at room temperature, followed by histological processing. Then, the samples were stained with hematoxylin and eosin (HE). Simultaneously, the ileum was fixed in 4% paraformaldehyde and subjected to histological processing. HE staining was performed, and pathological changes in the femurs, tibiae, and ileum postovarian removal were observed under a microscope.

Intestinal permeability test

The effects of various treatments on the integrity and permeability of the intestinal mucosal barrier were assessed with experiments involving the addition of lactulose and mannitol to the urine of living animals. High-performance liquid chromatography (HPLC) was used for the quantitative analysis of lactulose and mannitol

levels in the urine samples. Chromatograms for lactulose and mannitol were acquired and integrated with Xcalibur 3.0 software. Subsequently, linear regression analysis was performed with a weighting coefficient of $1/x^2$ to evaluate the observed effects.

ELISA

The wells of 96-well plates were prepared according to the kit instructions, and standard, sample, and blank wells were established. Then, the plate was prepared following the ELISA kit guidelines. We set the wavelength to 450 nm for the optimal measurement of the optical density (OD). The OD values in the standard wells were measured with an ELISA reader. Finally, a standard curve was established by plotting the OD values obtained from the standard wells. Standard curves were used to calculate the concentrations of IL-1, IL-6, and TNF-α in peripheral blood samples.

Cell isolation and culture

As previously described, BMSCs were isolated from the femurs of SD rats [29]. In brief, the femur and tibia were aseptically opened, and the bone marrow was flushed with α-MEM (SH30265.01; Cyclone, Logan, USA) supplemented with 1% penicillin–streptomycin (PS; p1400; Sorobio, Beijing, China). The epiphysis was removed, and the bone marrow cells were washed with α-MEM supplemented with 1% PS, followed by centrifugation. After the supernatants were discarded, the cells were resuspended in α-MEM supplemented with 1% PS and then cultured in α-MEM supplemented with 10% fetal bovine serum (FBS; 10,099,141; Gibco, Thermo Fisher Scientific, USA). After 24 h of initial cultivation, the culture medium was replaced with fresh and complete α-MEM to remove nonadherent cells. Adherent cells were cultured for 3–5 days and passaged when they reached 90% confluence.

Isolation and characterization of exosomes from BMSCs

We isolated EVs from BMSCs following a previously established protocol [30]. In brief, femoral BMSCs were isolated from SD rats and cultured. The BMSCs were characterized by flow cytometry (CD29+, CD38+, CD90+, and CD45+) and cultured in exosome-free medium for 72 h. The supernatants from the BMSC cultures were subsequently collected and centrifuged to eliminate dead cells or debris. The obtained culture supernatants were filtered through a 0.22-μm filter and subjected to ultracentrifugation at 100,000 × g for 4–6 h at 4 °C. The particles containing exosomes were washed with PBS and resuspended. NanoFCM was used to detect the EV surface proteins CD9 and CD81. The particle concentration was analyzed by NanoFCM, and the size distribution and morphology were examined by transmission electron microscopy (TEM) (Hitachi H7500 TEM).

BMSC-derived exosomal miRNA sequencing

RNA extraction from BMSC-derived exosomes was carried out with the ExoQuick® Exosome Isolation and RNA Purification Kit (EQ806TC-1; System Biosciences, Mountain View, USA). The integrity of the extracted RNA was assessed with an Agilent Bioanalyzer 2100 (Agilent Technologies, Palo Alto, USA). After RNA labeling and array hybridization, the Agilent Microarray Scanner was subsequently used to scan the slides with the default settings. The raw data were processed with the Agi Micro RNA R package. Differential miRNA expression analysis was performed on BMSC-derived exosomes from both the control group and the OVX group, and genes exhibiting an absolute fold change ≥ 1 and $P < 0.05$ were considered to be differentially expressed.

Quantitative RT–PCR

Quantitative RT–PCR analysis was conducted on the BMSCs, which were rapidly frozen with liquid nitrogen and stored at −80 °C. The frozen cells were crushed in liquid nitrogen, total RNA was extracted with TRIzol reagent. Relative changes in gene expression were analyzed with the $2^{-\Delta\Delta CT}$ method.

PCR primers:

Wnt3A F	CAGGAACTACGTGGAGATCATGC
Wnt3A R	CGTGTCACTGCGAAAGCTACT
Bmp2 F	TCTTCCGGGAACAGATACAGG
Bmp2 R	TGGTGTCCAATAGTCTGGTCA
Tgf-β F	GGGACATCAAACCTCTCTCAAC
Tgf-β R	GAGGACTGGCAGCTATGTAAAC
Runx2 F	AGAGTCAGATTACAGATCCCAGG
Runx2 R	TGGCTCTTCTTACTGAGAGAGG
Osterix (SP7) F	CCTACTTACCCGTCTGACTTTG
Osterix (SP7) R	CAACTGCCTTGGGCTTATAGA
Pparγ F	GACCTGAAGCTCCAAGAATACC
Pparγ R	TTCATGTGGCCTGTTGTAGAG

Osteogenic, adipogenic differentiation or cartilage induction of BMSCs

BMSCs were seeded at a density of 1×10^5 cells/well for osteogenic differentiation and at 2×10^5 cells/well for adipogenic differentiation in 48-well plates and cultured in complete medium for 24 h. Subsequently, osteogenic or adipogenic differentiation was induced with specific media (MUBMD-90021 or MUBMD-90031; Cyogen Biosciences). The differentiation medium was changed every two days. To analyze osteogenic or adipogenic gene

expression, the cells were collected 2 days after induction and subjected to qRT–PCR. To assess the formation of mineralized nodules or lipid droplets, osteogenesis or lipogenesis was induced for 14 and 21 days, respectively. Alizarin Red S (ARS) solution was used to assess osteogenic differentiation, while Oil Red O (ORO) staining was used to assess adipogenic differentiation. BMSCs were seeded at a density of 1×10^5 cells/well for cartilage induction. Alcian blue staining was used to assess cartilage induction.

Fecal microbial DNA extraction, amplification and sequencing

Fecal samples were collected in sterile EP tubes and immediately frozen at −80 °C for subsequent processing. Fecal microbial DNA was extracted with the QI Aamp Fecal DNA Mini Kit (Qiagen, Hilden, Germany). PCR amplification was conducted with a gradient PCR instrument (LongGene L96G, China). The V3-V4 region of the 16S rRNA gene was targeted in three independent PCRs with forward primers (341F, 5'-CCTACGGGNGGCGCG CGCAG-3') and reverse primers (805R, 5'-GACTAC HVGGTATCTAATCC-3'), and quantitative bacterial genomic DNA was used as the template. The replicated PCR products were then summarized, and the products were purified with Agencourt AMPure XP magnetic beads (Beckman Coulter, USA) with the Top Taq DNA Polymerase Kit (TransGen, China). The purity and concentration of the purified DNA samples were assessed with a NanoDrop 2000 spectrophotometer (Thermo Fisher Scientific, USA). Dual-end sequencing was performed with the HiSeq 2500 platform (Illumina, San Diego, CA, USA).

16S rRNA gene sequencing analysis

The dual-end data from the raw data were concatenated with overlay, and subsequent quality control and chimeric filtering steps were performed to generate high-quality clean data. DADA2 was used for denoising, utilizing the concept of ASVs to construct an OTU table. The final ASV feature table and feature sequences were obtained, enabling further analysis, including diversity analysis, species classification annotation, and differential analysis. Representative sequences were generated, and singletons were removed to produce the final OTU table. The Silva database was used for the classification of representative OTU sequences [31]. The assign Taxonomy function within the R software package DADA2 [32] was utilized for sequence classification. In the downstream analysis, feature tables, classification tables, representative sequences, phylogenetic trees, and metadata were imported and stored as phylogenetic library objects with the R package phylogenetic library [33].

Ruminococcus treatment

Ruminococcus torques Holdeman and Moore (BNCC341166) freeze-dried powder was obtained from the Be-Na Culture Collection and reconstituted in sterile physiological saline to create a bacterial solution at a concentration of 10^7 CFU/ml. The intervention was delivered to rats in the experimental group by oral gavage in an SPF environment, with a gavage dose of 2 ml administered over a period of 2 weeks. Throughout the experiment, each group of rats was given free access to food and water.

Immunohistochemistry (IHC) for Ki67

Rat femur and tibia paraffin sections were subjected to a sequence of procedures, including dewaxing, antigen retrieval, H_2O_2 treatment, and blocking with 5% bovine serum. Then, the sections were subjected to an overnight incubation with an anti-Ki67 antibody at 4 °C, followed by exposure to a biotinylated secondary antibody and the avidin–biotin horseradish peroxidase complex. After DAB visualization and hematoxylin counterstaining, the sections were visualized under a microscope, and images were analyzed with ImageJ software.

TUNEL assay

Femur and tibia paraffin sections were permeabilized with proteinase K, followed by incubation with a labeling buffer comprising biotin-conjugated dUTP and the enzyme TdT. Then, the sections were subjected to a reaction with FITC-conjugated streptavidin for 1 h at 37 °C, followed by counterstaining with DAPI in the dark. The sections were examined by fluorescence microscopy. Cells that emitted green fluorescence were identified as TUNEL-positive (apoptotic) cells, and the apoptosis index (%) was defined as the proportion of TUNEL-positive cells to the total cell count.

Statistical analysis

All the data are presented as the means ± standard deviations. Statistical comparisons between the control and OVX groups were conducted with Student's t test (SPSS Statistical Software). A significance threshold of $P<0.05$ was applied. Bonferroni-adjusted pairwise comparisons were performed to address multiple comparisons, specifically between the control OVX group and *Ruminococcus* + OVX group. The dataset was analyzed with one-way ANOVA, followed by Tukey's multiple test (SPSS Statistical Software), where a P value <0.05 was considered to indicate statistical significance.

Results

Alterations in intestinal permeability and bone density following ovariectomy in rats

To investigate the pivotal role of alterations in intestinal permeability in the bone loss that occurs due to ovariectomy, we examined pathological changes in both the gut and bones of ovariectomized rats. As shown in Fig. 1b, compared with the control, ovariectomy resulted in slender femurs, lighter staining, fewer trabeculae, and significantly increased spacing. The bone trabeculae in the tibial tissue exhibited significant reduction and slimness, accompanied by an increase in fat vacuole numbers and inflammatory cell infiltration. These findings indicate that ovariectomy induces bone loss and osteoporosis in rats. Furthermore, osteoporosis induced by bilateral ovariectomy did not cause notable changes in the thickness of the intestinal wall of the ileum. However, the intestinal villus height (VH) and the ratio of VH to crypt depth (VH/CD) in the OVX group were significantly lower than those in the control group, while the CD in the OVX group was significantly greater than that in the control group (Fig. 1c and d). In addition, we measured the concentrations of lactulose and mannitol in rat urine to evaluate the intestinal permeability of ovariectomized rats. The content of lactulose in the urine of ovariectomized rats was significantly greater than that of control rats ($P < 0.05$) (Fig. 1e). These data suggest that osteoporosis due to ovariectomy significantly impacts the integrity and permeability of the intestinal mucosal barrier. Ovariectomy-induced osteoporosis in rats was accompanied by a significant increase in peripheral blood TNF-α, IL-1, and IL-6 levels (Fig. 1f), which is possibly associated with alterations in the integrity and permeability of the intestinal mucosal barrier.

Ovariectomy-induced changes in the gut microbiota composition in rats

After filtering, quality control, and chimeric removal, a total of 1,054,679 sequences were obtained from the 16S rRNA gene sequencing data of 20 fecal samples, averaging 52,733 ± 4,640 sequences per sample (ranging from 45,375 to 62,614 sequences per sample). As shown in Fig. 2a, the control group included 4926 unique ASVs, the OVX group included 4294 unique ASVs, and 1491 ASVs

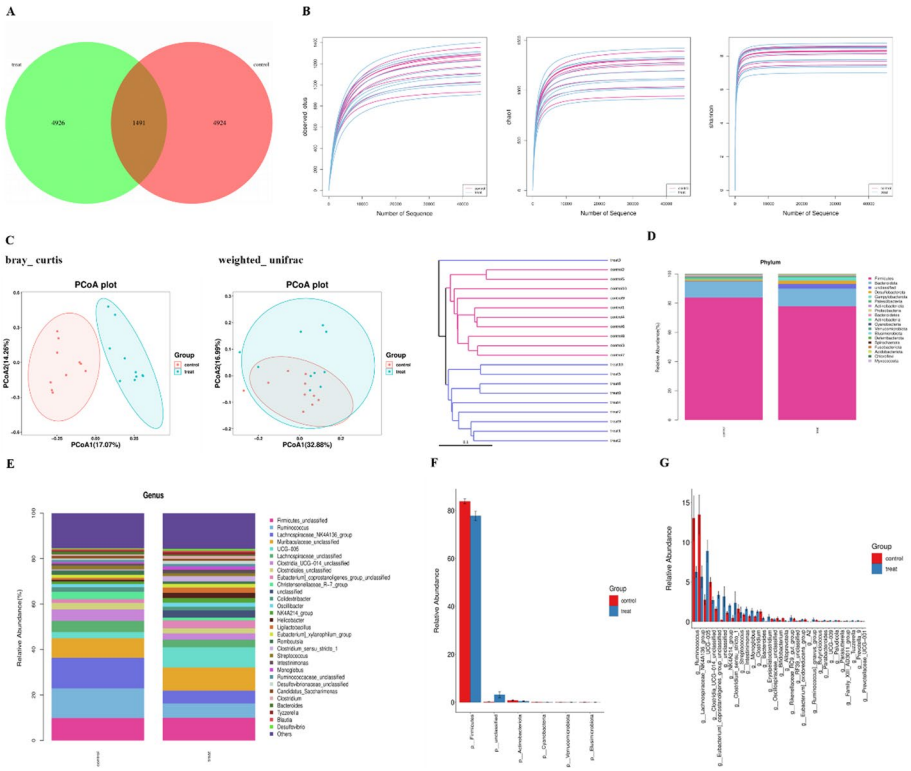

Fig. 2 Ovariectomy can lead to dysbiosis of the gut microbiota in rats. **a** Venn diagram analysis comparing the control and OVX groups. **b** Rarefaction curves illustrating alpha richness in the control and OVX groups. **c** Scatter plots showing the principal coordinate analysis (PCoA) of fecal microbial communities at the genus level, utilizing the Bray–Curtis distance and weighted UniFrac distance. **d** Composition of the gut microbiome at the phylum level. **e** Composition of the gut microbiome at the genus level. **f** Phylum-level composition of the gut microbiota of female rats, presented in bar graph format. **g** Genus-level composition of the gut microbiota of female rats, displayed in a bar graph. The data are expressed as the means ± SDs, $n = 10$ per group (A-G). Treated, OVX group

were shared between the two groups. To assess sequencing data adequacy and bacterial abundance characteristics, we performed sparse analysis and computed the observed OTU, Chao1, and Shannon indices. The saturation curves for each group approach saturation (Fig. 2b), confirming the robustness of the sequencing data with no detection of new species. This suggests that ovarian resection did not significantly impact the α diversity, species richness, or evenness of the gut microbiota in the two groups, as they remained comparable. Then, the β diversity was calculated at the genus level. The principal coordinate analysis (PCoA) results revealed distinct clusters between the control group and OVX group, with PCoA1 scores of 17.07% and PCoA2 scores of 14.55%. PCoA has a dominant impact on separation and clustering, whether it is based on the Bray–Curtis distance or the weighted_UniFrac distance (Fig. 2c). Furthermore, cluster analysis revealed distinct patterns between the control group and the OVX group, with robust clustering between the two groups (Fig. 2c). At the phylum level, as shown in Fig. 2d, *Firmicutes* and *Bacteroidetes* constituted the major components of the gut microbiota, collectively constituting more than 90% of the total gut microbiota in both the control and OVX groups. The abundance of *Firmicutes* tended to decrease in the OVX group whereas the abundance of *Bacteroidetes* tended to increase in the OVX group compared with the control group (Fig. 2f). 16S rRNA gene amplicon sequencing analysis revealed that at the genus level, the abundances of g_*Ruminococcus* and g_*Lachnospiraceae_NK4A136_group* were significantly decreased in the OVX group compared with the control group, whereas the abundance of *g_UCG-005* was increased (Fig. 2e and g). Among these three altered genera, *g_Ruminococcus* exhibited the most significant changes. Therefore, we speculate that the decreased abundance of *g_Ruminococcus* may contribute to osteoporosis in estrogen-deficient rats. Further exploration of the differential bacteria in *g_Ruminococcus* is warranted.

After ovariectomy: impact on the osteogenic and adipogenic differentiation of BMSCs

BMSCs were isolated from OVX model rats and observed by light microscopy. Primary BMSC cultures from the control and OVX groups contained densely clustered cells, with spindle-shaped cells extending from the central region. Continuous media exchange revealed comparable cell morphologies between the OVX and control groups, both of which presented whirlpool-like growth patterns (Fig. 3a). Although the control group exhibited a slightly greater growth rate and density under the same culture conditions, flow cytometry analysis of BMSC surface markers (CD34, CD29, CD45, and CD90) revealed positive expression of CD29 and CD90 and negative expression of CD23 and CD45 (Fig. S1); these results confirmed that the isolated cells were BMSCs. Then, Alizarin Red and ORO staining were performed at different time points during the induction of osteogenic differentiation in BMSCs from the OVX and control groups. Additionally, the expression of osteogenic- and adipogenic-related genes, including Runx2, Bmp2, Osterix, Tgf-β, Wnt3A, and Ppar-γ, was assessed. During the induction of osteogenic differentiation, spindle-shaped cells transitioned into irregular shapes, forming clustered structures in both the OVX and control groups. Alizarin Red staining revealed the development of calcium nodules, with the control group exhibiting greater numbers and densities of calcium nodules than the OVX group within the same induction cycle (14 or 21 days) (Fig. 3b). ORO staining revealed a significant increase in intracellular lipid droplet formation on the 14th day of adipogenic differentiation, with the number of lipid droplets gradually increasing over time. By the 21st day, the lipid droplets had fused with each other. Notably, the number and density of lipid droplets were greater in the BMSCs in the OVX group than in those in the control group during the same induction period (Fig. 3c). Gene expression analysis revealed that, compared with those in the control group, Ppar γ expression was significantly increased, whereas Tgf-β, Wnt, RunX2, and Osterix expression levels were significantly decreased in the OVX group after 14 and 21 days of osteogenic differentiation (Fig. 4c and e). Similarly, during adipogenic differentiation, Ppar γ expression was significantly increased, whereas Bmp2, Tgf-β, Wnt, Runx2, and Osterix expression levels were significantly decreased in the OVX group compared with the control group after 14 and 21 days ($P < 0.05$).

Characterization and miRNA profiling of exosomes from BMSCs

There are many mechanisms by which an altered microbiota can participate in the progression of osteoporosis, and among these mechanisms, a fundamental mechanism could involve the ability of the microbiome to regulate miRNA expression and function. Following the isolation and culture of exosomes derived from the BMSCs of ovariectomized rats, the morphology of these exosomes was examined by TEM, and the results revealed a distinctive cup-shaped structure (Fig. 4a). The size analysis indicated that these spherical nanoparticles had an approximate size of 75.89 ± 15.39 nm, which was consistent with the TEM findings (Fig. 4b). Flow cytometry analysis revealed a significant increase in surface marker expression, including CD9 and CD81 expression, on the isolated nanoparticles compared with the BMSCs (Fig. 4c); these results confirmed the successful isolation of exosomes from the BMSCs. Subsequent miRNA

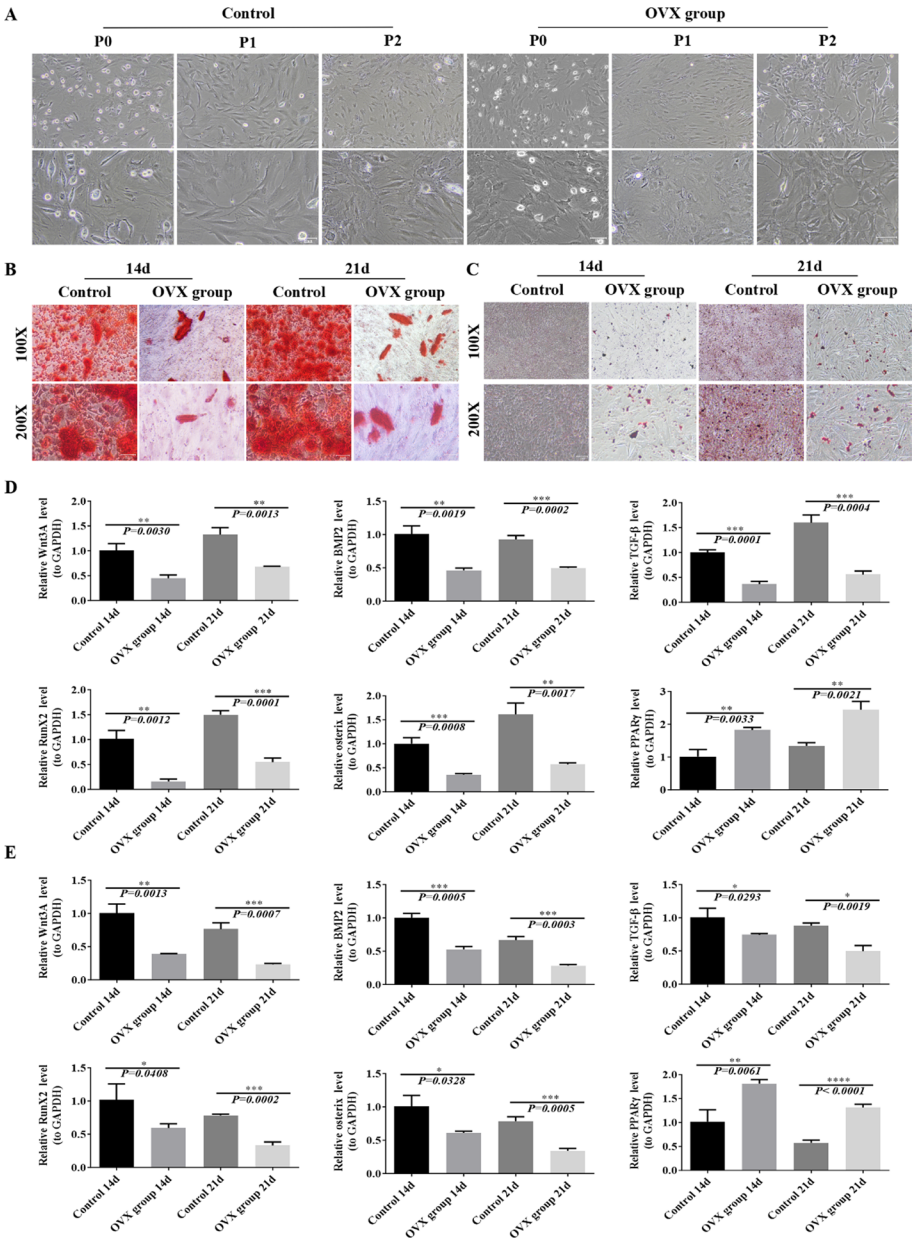

Fig. 3 Influence of ovarian removal on the osteogenic and adipogenic differentiation capacities of rat BMSCs. **a** Representative images of primary BMSCs from P0-P3. **b** Representative images of Alizarin Red S-stained BMSCs at 100X (upper) and 200X (lower) after 14 days and 21 days of osteogenic differentiation. **c** Representative images of ORO-stained BMSCs after 14 days and 21 days of adipogenic differentiation. **d**–**e** Wnt3A, Bmp2, Tgf-β, Runx2 Osterix and Pparγ mRNA expression in rat BMSCs from the control and OVX groups after 14 days and 21 days of osteogenic or adipogenic differentiation, respectively. $n = 6$

sequencing and bioinformatics analysis were conducted to reveal the comprehensive miRNA expression profile of these BMSC-derived exosomes. Table S1 shows the differential expression of miRNAs in the exosomes from osteoporotic rat BSMCs. A total of 28 miRNAs were differentially expressed, including 25 upregulated and 3 downregulated miRNAs ($P < 0.05$), as shown in Fig. 4d and e. Significant differences in miRNA expression ($|\log2FC| > 1$, $P < 0.05$) are summarized. Two miRNAs with significantly differential expression were selected for further analysis: miR-23b-3p, which was significantly upregulated, and miR-151-3p, which was significantly downregulated. Moreover, KEGG pathway annotation classification and enrichment analysis were performed

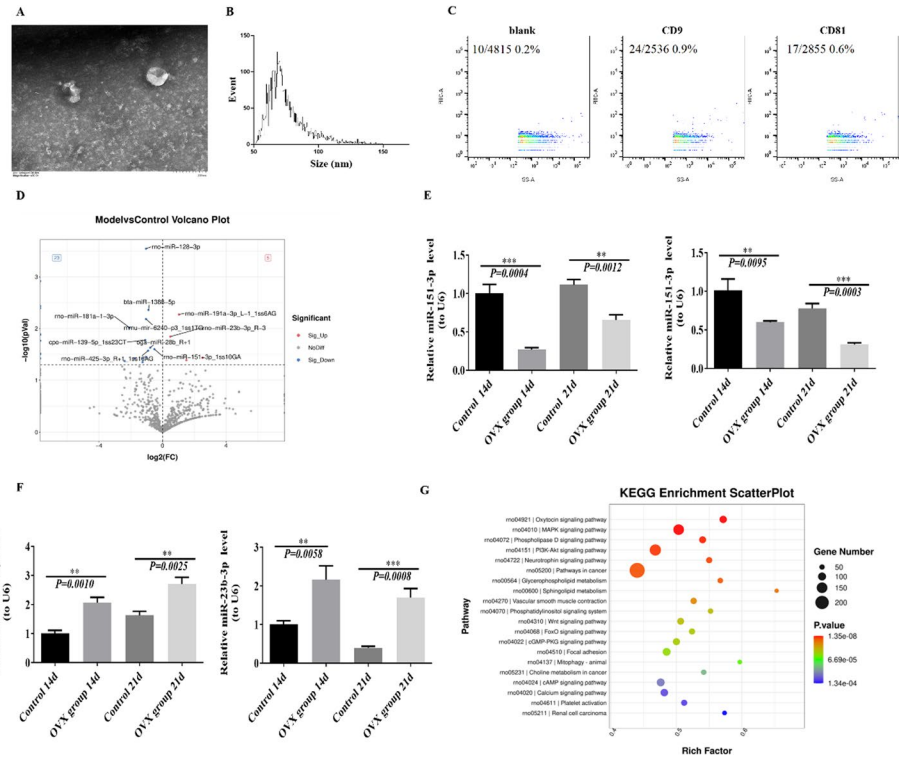

Fig. 4 Sequencing and bioinformatics analysis of BMSC-derived exosomal miRNAs. **a** Morphology of BMSC-derived exosomes. **b** Diameter distribution of BMSC-derived exosomes. **c** Exosomal marker analysis. **d** Volcano plot of differentially expressed miRNA analysis. **e**–**f** miRNA expression in BMSC-derived exosomes from the control and OVX groups after 14 days and 21 days of osteogenic or adipogenic differentiation, $n=6$. **g** KEGG enrichment analysis of genes associated with the BMSC-derived exosomal miRNAs

on the upregulated genes. Enrichment analysis was conducted with the phyper function in R software to calculate the *P* values, followed by FDR correction to obtain the Q values. Pathways that were significantly enriched in the differentially expressed genes included the oxytocin signaling pathway, the MAPK signaling pathway, the phospholipase D signaling pathway, and the PI3K-AKT signaling pathway. Examination of the enriched diseases within these pathways revealed associations with bone metabolism balance, osteoporosis, osteogenesis imperfecta, and osteosclerosis. These findings suggest that exosomal miR-23b-3p and miR-151-3p may influence the osteogenic differentiation of BMSCs by modulating the oxytocin, MAPK signaling, phospholipase D, and PI3K-Akt signaling pathways.

Influence of Ruminococcus on osteogenic differentiation in ovariectomized rats

Numerous experiments have also demonstrated the presence and functions of a microbiota–bone axis that can induce the onset of osteoporosis. To further identify changes in the gut microbiome that are caused by estrogen deficiency, we conducted LDA effect size (LEfSe) analysis to identify differences between the control and OVX groups. The results revealed a significant decrease in the relative abundance of *g_Lachnospiraceae_NK4A136* and *g_Ruminococcus*, whereas the abundance of *g_UCG_005* was significantly greater in the OVX group than in the control group (Fig. 5a and b). Histological examination of mouse colon tissue sections by HE staining revealed notable differences in the ileum between the two groups. Compared with the control group, the OVX group exhibited a significant reduction in intestinal VH and VH/CD, accompanied by inflammatory cell infiltration; however, there were no significant changes in intestinal wall thickness or crypt depth. In contrast, the OVX + *Ruminococcus* group presented marked increases in intestinal VH, CD, intestinal wall thickness, and VH/CD, which were accompanied by decreased inflammatory cell infiltration (Fig. 5c and d). Moreover, the ELISA results revealed that the OVX group had higher peripheral blood levels of IL-1, IL-6, and TNF-α than in the control group. Although the administration of *Ruminococcus* in the OVX + *Ruminococcus* group significantly increased the levels of these inflammatory markers compared with those in the control group, the levels of these markers were significantly lower than those in the OVX group ($P<0.05$) (Fig. 5e).

The observed pathological changes in the intestine might be associated with increased peripheral blood inflammation. Furthermore, bone density analysis revealed a significant decrease in bone mineral density (BMD) in the OVX group compared with the control group. Notably, after *Ruminococcus* administration, the BMD value of OVX model rats slightly increased ($P<0.05$), and the bone density value was comparable to that of the control group (Fig. 5f). Further examination of the femurs and tibiae from OVX model rats revealed a decrease in numbers of bone trabeculae, increased numbers of fat vacuoles, and increased numbers of inflammatory cells. However, following the administration of *Ruminococcus*, the numbers of bone trabeculae were ameliorated, the numbers of fat vacuoles were reduced, and the numbers of inflammatory cells were decreased in the femur and tibia tissues (Fig. 5g and h). Moreover, inducing the osteogenic and adipogenic differentiation of BMSCs for 14 and 21 days resulted in distinct outcomes. Alizarin Red staining revealed that the degree of osteogenic differentiation in the OVX group was significantly lower than that in the control group. In contrast, *Ruminococcus* administration to OVX model rats significantly increased the degree of osteogenic differentiation, indicating a notable effect on alleviating the inhibition caused by ovariectomy (Fig. 5i). Furthermore, ORO staining revealed that the degree of adipogenic differentiation in the OVX group was notably greater than that in the control group. Treatment with *Ruminococcus* substantially mitigated the degree of adipogenic differentiation in ovariectomized rats, highlighting its significant effect on alleviating the OVX-induced increase in adipogenic differentiation (J). Finally, an examination of genes related to osteogenesis and adipogenic differentiation revealed significant increases in miR-23b-3p and Pparγ expression in the OVX group compared with the control group. However, after *Ruminococcus* intervention, the expression of miR-23b-3p and Pparγ was reduced. Ovariectomy in rats significantly decreased the expression of miR-151-3p, Bmp2, and Tgf-β, as well as that of Wnt3A, Runx2, and Osterix. However, *Ruminococcus* increased miR-151-3p, Bmp2, Tgf-β, Wnt3A, Runx2, and Osterix expression (Fig. S2). Thus, treatment with *Ruminococcus* alleviated the changes in the expression of genes related to osteogenesis and adipogenesis induced by osteoporosis.

The proliferation and live/dead status of BMSCs from rats transplanted with Ruminococcus

As show in Fig. 6, TUNEL assay results revealed that the number of TUNEL-positive cells was increased in both the femurs and tibiae of OVX model rats, indicating increased apoptosis of the BMSCs in OVX model rats (Fig. 6a, b and e). In contrast, compared with the OVX alone, *Ruminococcus* led to a significant decrease in the numbers of TUNEL-positive cells, reflecting BMSC resistance to apoptosis. IHC results (Fig. 6c, d and f) revealed lower Ki67 expression in the femurs and tibiae of OVX model rats than in those of normal rats, indicating decreased BMSC proliferation in the OVX group. However, *Ruminococcus* markedly increased Ki67 expression, highlighting its effects on promoting BMSC proliferation in OVX model rats.

Effect of exosomes from BMSCs on osteogenic, adipogenic differentiation and cartilage induction in ovariectomized rats

As shown in Fig. S3 (a-d and m), compared with the BMSC group, the BMSC + EXO group exhibited a significant increase in calcium salt deposition. In contrast, the BMSC + EXO (OVX) group showed a significant decrease in calcium salt deposition compared to the BMSC + EXO group. Moreover, the BMSC + EXO (OVX) group demonstrated a significant increase in calcium salt deposition compared to the BMSC + EXO (OVX + *Ruminococcus*) group. Additionally, compared to the BMSC group, the BMSC + EXO (OVX) group exhibited a significant decrease in calcium salt deposition, while the BMSC + EXO (OVX + *Ruminococcus*) group showed a significant increase in calcium salt deposition. In terms of adipogenic differentiation, as shown in Fig. S3 (e–h and *n*), compared with the BMSC group, the BMSC + EXO group exhibited a significant increase in fat content. However, compared to the BMSC + EXO group, the BMSC + EXO (OVX) group showed a significant decrease in fat content. The BMSC + EXO (OVX) group also exhibited a significant

(See figure on next page.)

Fig. 5 *Ruminococcus* administration ameliorates osteoporosis caused by ovarian removal in rats. **a** Cladogram showing taxa enriched in the control (red) and treatment (green) groups. Yellow nodes indicate non-significant taxa. **b** LDA score plot illustrating taxa with significant differences. Bar length represents effect size, with red indicating enrichment in the control group and green in the treatment group. **c** Pathological changes in the ileum at 100X (upper) and 200X (lower) magnification after *Ruminococcus* administration. **d** Measurements of the ileal wall thickness, villus height, crypt depth, and the ratio of villus height to crypt depth. The data are expressed as the means ± SDs. $n=6$ per group. **e** Peripheral blood IL-1, IL-6, and TNF-α levels after *Ruminococcus* administration. The data are expressed as the means ± SDs. $n=10$ per group. **f** Assessment of bone density in rats after *Ruminococcus* administration. **g–h** Pathological changes in the femur and tibia observed at 100X (upper) and 200X (lower) magnifications after *Ruminococcus* administration. **i** Representative images of Alizarin Red S-stained BMSCs at 100X (upper) and 200X (lower) after 14 days and 21 days of osteogenic differentiation. **j** Representative images of ORO-stained BMSCs at 100X (upper) and 200X (lower) after 14 days and 21 days of osteogenic differentiation

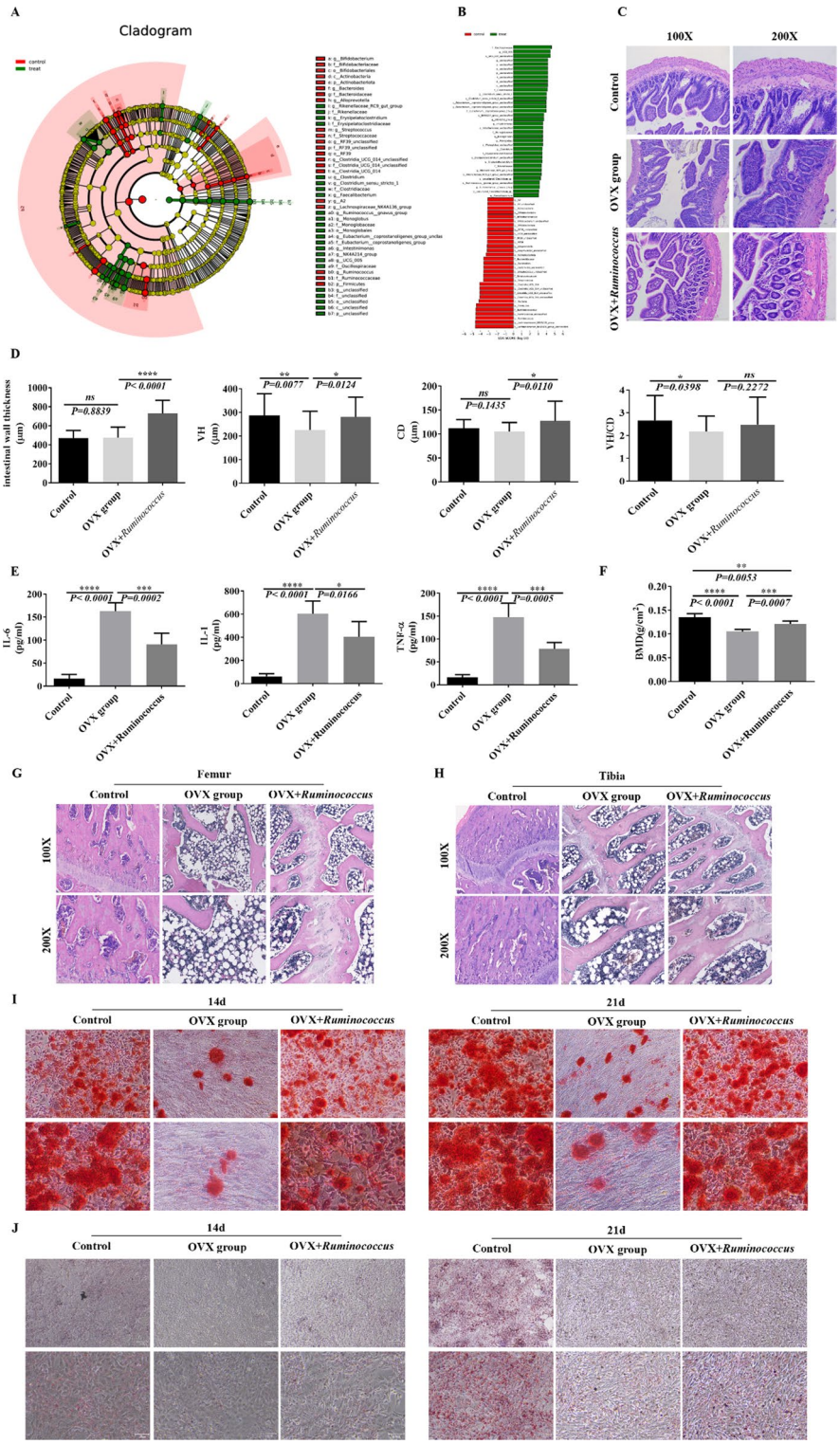

Fig. 5 (See legend on previous page.)

increase in fat content compared to the BMSC + EXO (OVX + *Ruminococcus*) group. Additionally, compared with the BMSC group, the BMSC + EXO (OVX) group showed a significant decrease in fat content, while the BMSC + EXO (OVX + *Ruminococcus*) group exhibited a significant increase in fat content. Finally, regarding

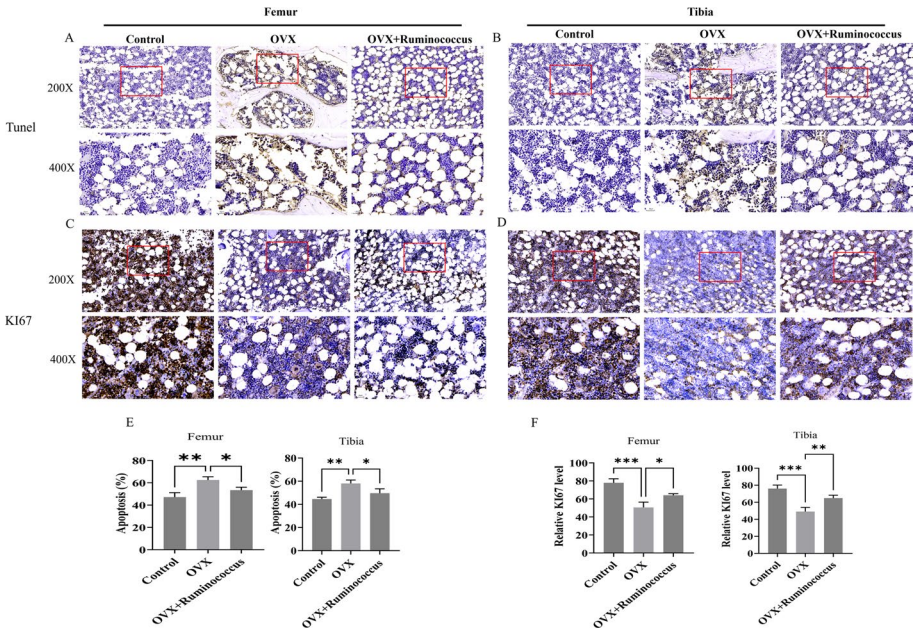

Fig. 6 *Ruminococcus* increased Ki67 expression and decreased apoptosis in the femurs and tibiae of OVX model rats. **a**, **b** and **e** TUNEL assay to assess femur and tibia apoptosis (400 × and 200 ×) and quantitative percentages of TUNEL-positive cells, i.e., the apoptosis index ($n = 3$). **c**, **d** and **f** IHC analysis of Ki67 expression in femurs and tibiae (400 × and 200 ×) and quantitative percentages of Ki67-positive cells ($n = 3$). The data represent the means ± SDs. *$p < 0.05$

chondrogenic differentiation, as shown in Fig. S3 (i-l and o), the acidic mucopolysaccharide content was significantly higher in the BMSCs + EXO group compared to the BMSCs group. The difference was statistically significant. In contrast, the BMSCs + EXO (OVX) group showed a significant decrease in acidic mucopolysaccharide content compared to the BMSCs + EXO group. The BMSCs + EXO (OVX) group also exhibited a significant increase in acidic mucopolysaccharide content compared to the BMSCs + EXO (OVX + *Ruminococcus*) group, with the difference being statistically significant. Compared with the BMSCs group, the BMSCs + EXO (OVX) group showed a significant decrease in acidic mucopolysaccharides, while the BMSCs + EXO (OVX + *Ruminococcus*) group showed a significant increase in acidic mucopolysaccharides, with the difference being statistically significant.

Discussion

The gut microbiota is closely associated with various metabolic diseases, such as NAFLD, inflammatory bowel disease, and rheumatoid arthritis [34–36]. Crohn's disease (CD), ulcerative colitis (UC), and pouchitis are chronic, multifactorial inflammatory bowel diseases (IBD) consistently linked to gut microbial dysbiosis. Increasing studies suggest a positive association between *Ruminococcus g* and IBD, although a causal relationship remains to be proven [37]. Irritable bowel syndrome (IBS) is another chronic, heterogeneous disorder, affecting approximately 6% of the population. Its pathophysiology is multifactorial, with an altered gut microbiota believed to play a significant role. Stool and colon biopsy samples from IBS patients and healthy controls, as well as from a mouse model of IBD induced by 2,4,6-trinitrobenzene sulfonic acid (TNBS), show that the severity of symptoms and inflammation are likely linked to changes in mucus-associated bacteria such as *Ruminococcus g* [38]. *Ruminococcus g has also been consistently associated with features of metabolic syndrome in humans, including increased body fat percentage, as shown in a large cohort study (n = 2875) and two replication cohorts (n = 999 and n = 1341) in Norway, involving participants aged 20–94 years* [39]. Beyond the diseases mentioned, *Ruminococcus g* has been implicated in a variety of other conditions. While its precise mechanisms are not fully understood, its therapeutic potential is widely recognized. Numerous studies have highlighted the pivotal role of the gut microbiota in bone metabolism [10, 36, 40].

In this study, we induced osteoporosis in rats by performing ovariectomy and observed a significant increase in intestinal permeability. The proportions of *Firmicutes* and *Bacteroidetes* in the lower intestinal lumen increased, and substantial differences in the gut microbiota of the groups were observed. Consequently, we hypothesize that the disruption of the gut microbiota induced by ovarian resection might contribute to bone loss in rats.

This hypothesis was supported by pathological sections, which revealed a marked reduction in trabeculae in the femur and tibia, accompanied by an increase in fat vacuole numbers and inflammatory cell infiltration after ovariectomy. Additionally, systemic inflammatory factors are known to play pivotal roles in bone homeostasis [41]. Our findings revealed significant increases in the peripheral blood levels of IL-1, IL-6, and TNF-α after ovarian resection.

The pathogenesis of osteoporosis involves numerous factors and complex connections, and the aging of BMSCs plays a pivotal role. Previous studies have definitively established that advanced glycation end products (AGEs) inhibit mitochondrial autophagy, suppress BMSC osteogenic differentiation, promote BMSC adipogenic differentiation, induce BMSC aging, and expedite osteoporosis onset and progression [42]. In our present study, we isolated primary BMSCs from the femurs of ovariectomized rats. Following osteogenic and adipogenic differentiation, there was a discernible reduction in the degree of BMSC osteogenic differentiation, which was accompanied by an increase in adipogenic differentiation. The delicate equilibrium between osteogenesis and adipogenic differentiation plays a pivotal role in osteoporosis initiation and progression. BMSC-derived exosomal miRNAs may closely regulate target genes that are involved in osteogenic and adipogenic differentiation, thereby exerting a crucial effect on this process. EVs are key players in intercellular communication by facilitating the transfer of bioactive components, such as proteins, mRNAs, miRNAs, and genomic DNA, to recipient cells [43–45]. Bone matrix vesicles, which are nanoscale exosomes that are found within the bone matrix, have emerged as initial sites for bone mineralization, further highlighting their critical role in this complex process. Furthermore, a recent investigation demonstrated that exosomes from BMSCs are typically integrated into the bone matrix and released during bone resorption by osteoclasts, exerting time-dependent regulatory effects on bone homeostasis and vascular calcification [46]. EVs derived from immature BMSCs can promote osteogenesis and bone formation. However, the efficacy of aged BMSC-derived exosomes in promoting bone formation is diminished. Intriguingly, in vitro, these exosomes can enhance the adipogenesis of BMSCs and the mineralization of vascular smooth muscle cells (VSMCs). In vivo, these exosomes contribute to the imbalance in bone fat and induce vascular calcification in the presence of vitamin D3 or glandular induction [46]. Moreover, the miRNA regulatory target genes encapsulated within BMSC-derived exosomes may play a role in inducing the osteogenic and adipogenic differentiation of BMSCs, potentially representing a key pathway by which estrogen deficiency induces osteoporosis. miRNAs, which are a class of small noncoding RNAs, modulate cellular functions by downregulating target gene expression [47, 48]. Notably, miR-483-5p has been reported to positively regulate PPARγ, promoting adipogenesis in 3T3-L1 mouse preadipocytes through its expression [49]. Additionally, miR-483-5p can increase PPARγ expression by directly inhibiting the ERK1 gene, thereby promoting the adipogenic differentiation of human adipose-derived MSCs [50]. Another miRNA, namely, miR-2861, targets histone deacetylase 5 (HDAC5) to stimulate Runx2 expression, consequently promoting the osteoblast differentiation and osteogenic transdifferentiation of VSMCs [51, 52]. In our study, we isolated and extracted BMSC-derived exosomes and sequenced the miRNAs within them. The primary BMSC-derived exosomes from estrogen-deficient rats exhibited differential expression of miR-23b-3p and miR-151-3p, which are implicated in major signaling pathways, such as the oxytocin signaling pathway, the MAPK signaling pathway, the phospholipase D signaling pathway, and the PI3K–Akt signaling pathway. These distinct signaling pathways may be closely involved in maintaining the balance of bone metabolism and contributing to conditions such as osteoporosis, osteogenesis imperfecta, and osteosclerosis.

Dysbiosis of the gut microbiota contributes to various pathways that are involved in the progression of osteoporosis. Among these pathways, the regulation of miRNA expression and functional changes by the gut microbiota are key mechanisms underlying osteoporosis occurrence and development [11]. Therefore, this study proposes that the induction of osteoporosis due to estrogen deficiency may be mediated by changes in the gut microbiota, which regulate the expression of miRNAs in BMSC-derived exosomes. In our investigation, we revealed change in the abundance of *Ruminococcus* in estrogen-deficient rats. *Ruminococcus*, which is a crucial member of the rumen microbiota, is known for its potential probiotic capabilities related to cellulose degradation and short-chain fatty acid (SCFA) production [53, 54]. Studies on the gut–bone axis have indicated that healthy individuals have a greater abundance of *Ruminococcus* than patients with osteoporosis [55, 56]. Interestingly, in this study, we observed a significant reduction in the abundance of the gut genus *Ruminococcus* in female rats after ovariectomy. Notably, *Ruminococcus* may serve as a potential probiotic. Therefore, we hypothesize that *Ruminococcus* might be associated with mitigating osteoporosis. To explore this hypothesis, *Ruminococcus* was administered to estrogen-deficient rats. The results demonstrated that after the administration of *Ruminococcus*, the intestinal VH, CD, intestinal wall thickness, and VH/CD of the treated rats were significantly increased, whereas the number

of inflammatory cells was decreased. Moreover, peripheral blood levels of inflammatory factors were decreased, bone mass was restored to a certain extent, and the number of bone trabeculae in femoral tissue were increased, with reductions in fat vacuole and inflammatory cell numbers. At the cellular level, *Ruminococcus* ameliorated the changes in BMSC osteogenic and adipogenic differentiation caused by estrogen deficiency. The balance between the osteogenic and adipogenic differentiation of BMSCs is a crucial factor in maintaining bone mass. These findings suggest that *Ruminococcus* has the potential to ameliorate intestinal damage caused by estrogen deficiency. We hypothesize that *Ruminococcus* can ameliorate osteoporosis in estrogen-deficient rats by regulating the gut–bone axis. Although the specific mechanism of action in this pathway is not yet clear, our findings indicate that after the administration of *Ruminococcus*, there was a significant upregulation of miR-23b-3p and a downregulation of miR-151-3p in the exosomes of primary BMSCs from estrogen-deficient rats. These findings suggest that *Ruminococcus* may ameliorate the imbalance in osteogenic/adipogenic differentiation caused by estrogen deficiency by regulating BMSC-derived exosomal miR-23b-3p and miR-151-3p levels.

While potential miRNA targets of *Ruminococcus* have been identified, a deeper understanding of the underlying mechanisms is imperative. Given that bones are shielded from direct contact with the external environment and typically lack normal habitation by various microorganisms, we hypothesize that *Ruminococcus* might indirectly regulate BMSC-derived exosomal miRNAs, consequently influencing bone metabolism, through its metabolites or secreted factors. Further validation analysis will aim to investigate the impact of *Ruminococcus* metabolites or secreted factors on BMSC-derived exosomal miRNAs in hormone-deficient rats and to elucidate the pathways by which *Ruminococcus* modulates BMSC-derived exosomal miRNAs, such as those influencing autophagy or energy metabolism. This approach has the potential to increase our understanding of the mechanisms by which *Ruminococcus* contributes to ameliorating osteoporosis in estrogen-deficient rats.

In this study, we observed that probiotic intervention significantly regulated the multipotent differentiation ability of BMSCs in the ovariectomy (OVX) rat model through extracellular vesicles, specifically affecting osteogenic, adipogenic, and chondrogenic differentiation. During osteogenic induction, BMSCs in the OVX group showed lower calcium deposition, indicating impaired bone metabolism and reduced osteogenic potential. In contrast, the calcium deposition in the BMSCs + EXO (OVX + *Ruminococcus*) group significantly increased, suggesting that the *Ruminococcus* strain restored the osteogenic potential of BMSCs by regulating the intestinal microenvironment or immune response.

Gene expression analysis revealed that key osteogenic genes, such as Runx2, Bmp2, Osterix, Tgf-β, and Wnt3A, were significantly reduced in OVX group BMSCs during osteogenic differentiation, which aligns with the bone metabolism disorder observed in osteoporosis [57]. Additionally, during adipogenesis, BMSCs in the OVX group exhibited increased fat droplet formation, with a significant upregulation of Ppar-γ, indicating a tendency for BMSCs to differentiate into adipocytes. Gene expression analysis further supported this, showing a significant decrease in osteogenic-related genes such as Tgf-β, Wnt, Runx2, and Osterix under adipogenesis induction, while upregulation of Ppar-γ was identified as the primary driver of adipogenic differentiation [58]. Interestingly, the BMSCs + EXO (OVX + *Ruminococcus*) group, following *Ruminococcus* intervention, also displayed a higher number of fat droplets during adipogenic differentiation. This suggests that probiotics may regulate the balance between adipogenesis and osteogenesis, helping to prevent extreme imbalances between bone and lipid metabolism.

Furthermore, changes in acidic mucopolysaccharides reflect alterations in cartilage differentiation. In the OVX model, BMSCs showed reduced cartilage matrix synthesis, while extracellular vesicle intervention significantly increased the expression of chondrogenic-related genes. This suggests that extracellular vesicles may help restore balance between osteogenic, adipogenic, and chondrogenic differentiation pathways by regulating BMSC differentiation [59].

Overall, probiotic intervention plays a crucial role in regulating the multidirectional differentiation of BMSCs through extracellular vesicles, particularly in models of osteoporosis or similar diseases. This offers potential for restoring osteogenic function and opens new avenues for treating osteoporosis and lipid metabolism disorders by modulating the gut microbiota through stem cell therapy.

Conclusions

In summary, our study reveals the potential of oral *Ruminococcus* administration to alleviate osteoporosis and restore the disrupted balance between the osteogenic and adipogenic differentiation of BMSCs from OVX model rats. The observed changes in the expression of miR-23b-3P and miR-151-3p within BMSC-derived exosomes after *Ruminococcus* intervention suggest a regulatory role in the expression of key genes that are associated with the osteogenic and adipogenic differentiation of BMSCs. These findings suggest that *Ruminococcus* can mitigate ovariectomy-induced osteoporosis by modulating miR-23b-3p and miR-151-3p expression. Our study provides

new directions for exploring the potential of modulating the gut–bone axis in the treatment and prevention of osteoporosis. While we discovered that *Ruminococcus* can mitigate ovariectomy-induced osteoporosis by modulating miR-23b-3p and miR-151-3p expression, there are certain limitations related to the elucidation of the causal mechanisms and the determination of the impact of the gut microbiota–bone axis on osteoporosis. First, it is imperative to elucidate the pivotal components that govern the regulation of BMSC-derived exosomal miR-23b-3p and miR-151-3p by *Ruminococcus*. Second, further exploration of the target genes of miR-23b-3p and miR-151-3p is warranted, as are related mechanistic pathway studies.

Abbreviations

BMD	Bone mineral density
BMSCs	Bone marrow mesenchymal stem cells
CD	Crohn's disease
EVs	Extracellular vehicles
F/B ratio	*Firmicutes* To *Bacteroidetes* ratio
IBD	Inflammatory bowel diseases
IBS	Irritable bowel syndrome
IL-1β	Interleukin-1 beta
MSCs	Mesenchymal stromal cells
ORO	Oil Red O
OVX	Ovariectomy
SCFA	Short-chain fatty acid
SD	Sprague–Dawley
TEM	Transmission electron microscopy
TNF-α	Tumor necrosis factor-alpha
UC	Ulcerative colitis
VH/CD	Villus height to crypt depth

Supplementary Information

The online version contains supplementary material available at https://doi.org/10.1186/s13287-025-04256-y.

Supplementary material 1.

Supplementary material 2.

Supplementary material 3.

Acknowledgements
Not applicable. The authors declare that they have not used AI-generated work in this manuscript.

Author contributions
ZHY: Conceptualization, Writing Review & Editing, Methodology, Data Curation, Funding Acquisition. ZXJ: Conceptualization, Methodology, Writing Review & Editing, Data Curation. HB: Methodology, Investigation, Writing Original draft preparation, Visualization. SXL: Methodology, Investigation, Writing Original draft preparation. LF: Methodology, Investigation, Resources. XHY: Investigation, Writing. FXQ: Investigation, Resources. WZH: Investigation, Resources. GXP: Investigation, Resources. FY: Investigation, Resources. LGH: Investigation, Resources. All the authors have read and approved the final manuscript.

Funding
This study was supported by the General Project of Yunnan Basic Research Program (202301AT070104), the Joint Project of Kunming Medical University and Science and Technology Department of Yunnan Province (202101AY070001-119), the Yunnan Clinial Center for Emergency traumatic diseases (YWJZCSXJBYXZX), the Central guidance for local projects of HeBei province (246Z7718G).

Availability of data and materials
The sequencing data supporting the results of this study are available in the Sequence Read Archive (SRA) under the accession number [PRJNA1226085]. Additional data and materials can be made available upon reasonable request from the corresponding author.

Declarations

Ethics approval and consent to participate
The study titled "The Mechanism of Gut Microbiota Regulating the Osteogenic Differentiation Pathway of Bone Marrow Mesenchymal Stem Cells to Improve Osteoporosis and Fracture Healing" was approved by the Ethics Committee of the First Affiliated Hospital of Kunming Medical University (Approval No. kmmu20210178, Approval Date: March 2, 2022). Written informed consent was obtained from the guardian of each participant.

Consent for publication
Not applicable.

Competing interests
The authors declare that they have no known competing financial interests or personal relationships that could have appeared to influence the work reported in this paper.

Author details
[1]School of Public Health, North China University of Science and Technology, 21 Bohai Road, Cao Fei Dian, Tangshan 063210, Hebei, China. [2]International Science & Technology Cooperation Base of Geriatric Medicine, Tangshan 063210, Hebei, China. [3]Engineering Research Center of Bone and Joint Precision Medicine, Ministry of Education, Department of Orthopaedics, Beijing Key Laboratory of Spinal Disease Research, Peking University Third Hospital, Beijing 100191, China. [4]Department of Orthopedics, The First Affiliated Hospital of Kunming Medical University, Kunming 650032, Yunnan, China.

Received: 10 April 2024 Accepted: 27 February 2025
Published online: 18 March 2025

References

1. Chen C-Y, Rao S-S, Yue T, Tan Y-J, Yin H, Chen L-J, Luo M-J, Wang Z, Wang Y-Y, Hong C-G, Qian Y-X, He Z-H, Liu J-H, Yang F, Huang F-Y, Tang S-Y, Xie H. Glucocorticoid-induced loss of beneficial gut bacterial extracellular vesicles is associated with the pathogenesis of osteonecrosis. Sci Advan. 2022. https://doi.org/10.1126/sciadv.abg8335.
2. Zhang YW, Cao MM, Li YJ, Dai GC, Lu PP, Zhang M, et al. The regulative effect and repercussion of probiotics and prebiotics on osteoporosis: involvement of brain-gut-bone axis. Crit Rev Food Sci Nutr. 2023;63:7510–28.
3. Morais LH, Schreiber HL, Mazmanian SK. The gut microbiota–brain axis in behaviour and brain disorders. Nat Rev Microbiol. 2021;19(4):241–55. https://doi.org/10.1038/s41579-020-00460-0.
4. Wastyk HC, Fragiadakis GK, Perelman D, Dahan D, Merrill BD, Yu FB, et al. Gut-microbiota-targeted diets modulate human immune status. Cell. 2021;184:4137-53.e14.
5. Budden KF, Gellatly SL, Wood DL, Cooper MA, Morrison M, Hugenholtz P, et al. Emerging pathogenic links between microbiota and the gut-lung axis. Nat Rev Microbiol. 2017;15:55–63.
6. Zaiss MM, Jones RM, Schett G, Pacifici R. The gut-bone axis: how bacterial metabolites bridge the distance. J Clin Invest. 2019;129:3018–28.
7. Liu JH, Chen CY, Liu ZZ, Luo ZW, Rao SS, Jin L, et al. Extracellular vesicles from child gut microbiota enter into bone to preserve bone mass and strength. Adv Sci (Weinh). 2021;8:2004831.
8. Santos-Marcos JA, Rangel-Zuñiga OA, Jimenez-Lucena R, Quintana-Navarro GM, Garcia-Carpintero S, Malagon MM, et al. Influence of gender and menopausal status on gut microbiota. Maturitas. 2018;116:43–53.

9. Guan Z, Luo L, Liu S, Guan Z, Zhang Q, Li X, et al. The role of depletion of gut microbiota in osteoporosis and osteoarthritis: a narrative review. Front Endocrinol (Lausanne). 2022;13: 847401.
10. Lorenzo J. From the gut to bone: connecting the gut microbiota with Th17 T lymphocytes and postmenopausal osteoporosis. J Clin Invest. 2021;131: e146619.
11. Reyes A, Blanton LV, Cao S, Zhao G, Manary M, Trehan I, et al. Gut DNA viromes of Malawian twins discordant for severe acute malnutrition. Proc Natl Acad Sci USA. 2015;112:11941–6.
12. Chen R, Liao X, Chen F, Wang B, Huang J, Jian G, et al. Circulating microRNAs, miR-10b-5p, miR-328-3p, miR-100 and let-7, are associated with osteoblast differentiation in osteoporosis. Int J Clin Exp Pathol. 2018;11:1383–90.
13. Bianco P, Robey PG, Simmons PJ. Mesenchymal stem cells: revisiting history, concepts, and assays. Cell Stem Cell. 2008;2:313–9.
14. Pittenger MF, Discher DE, Péault BM, Phinney DG, Hare JM, Caplan AI. Mesenchymal stem cell perspective: cell biology to clinical progress. NPJ Regen Med. 2019;4:22.
15. Ciuffreda MC, Malpasso G, Musarò P, Turco V, Gnecchi M. Protocols for in vitro differentiation of human mesenchymal stem cells into osteogenic, chondrogenic and adipogenic lineages. Methods Mol Biol. 2016;1416:149–58.
16. Chen S, Chen X, Geng Z, Su J. The horizon of bone organoid: a perspective on construction and application. Bioact Mater. 2022;18:15–25.
17. Chen J, Li M, Liu AQ, Zheng CX, Bao LH, Chen K, et al. Gli1(+) cells couple with type H vessels and are required for type H vessel formation. Stem Cell Rep. 2020;15:110–24.
18. Yang N, Wang G, Hu C, Shi Y, Liao L, Shi S, et al. Tumor necrosis factor α suppresses the mesenchymal stem cell osteogenesis promoter miR-21 in estrogen deficiency-induced osteoporosis. J Bone Miner Res. 2013;28:559–73.
19. Du D, Zhou Z, Zhu L, Hu X, Lu J, Shi C, et al. TNF-α suppresses osteogenic differentiation of MSCs by accelerating P2Y(2) receptor in estrogen-deficiency induced osteoporosis. Bone. 2018;117:161–70.
20. Russell T, Watad A, Bridgewood C, Rowe H, Khan A, Rao A, et al. IL-17A and TNF modulate normal human spinal entheseal bone and soft tissue mesenchymal stem cell osteogenesis, adipogenesis, and stromal function. Cells. 2021;10:341.
21. Song H, Li X, Zhao Z, Qian J, Wang Y, Cui J, et al. Reversal of osteoporotic activity by endothelial cell-secreted bone targeting and biocompatible exosomes. Nano Lett. 2019;19:3040–8.
22. Hu Y, Li X, Zhang Q, Gu Z, Luo Y, Guo J, et al. Exosome-guided bone targeted delivery of Antagomir-188 as an anabolic therapy for bone loss. Bioact Mater. 2021;6:2905–13.
23. Liu H, Zhang Q, Wang S, Weng W, Jing Y, Su J. Bacterial extracellular vesicles as bioactive nanocarriers for drug delivery: advances and perspectives. Bioact Mater. 2022;14:169–81.
24. Qiu M, Zhai S, Fu Q, Liu D. Bone marrow mesenchymal stem cells-derived exosomal MicroRNA-150-3p promotes osteoblast proliferation and differentiation in osteoporosis. Hum Gene Ther. 2021;32:717–29.
25. Bhushan R, Grünhagen J, Becker J, Robinson PN, Ott CE, Knaus P. miR-181a promotes osteoblastic differentiation through repression of TGF-β signaling molecules. Int J Biochem Cell Biol. 2013;45:696–705.
26. Hassan MQ, Maeda Y, Taipaleenmaki H, Zhang W, Jafferji M, Gordon JA, et al. miR-218 directs a Wnt signaling circuit to promote differentiation of osteoblasts and osteomimicry of metastatic cancer cells. J Biol Chem. 2012;287:42084–92.
27. Lu GD, Cheng P, Liu T, Wang Z. BMSC-derived exosomal miR-29a promotes angiogenesis and osteogenesis. Front Cell Dev Biol. 2020;8: 608521.
28. Chen Y, Yokozeki H, Katagiri K. Physiological and functional changes in the stratum corneum restored by oestrogen in an ovariectomized mice model of climacterium. Exp Dermatol. 2017;26:394–401.
29. Zhu H, Guo ZK, Jiang XX, Li H, Wang XY, Yao HY, et al. A protocol for isolation and culture of mesenchymal stem cells from mouse compact bone. Nat Protoc. 2010;5:550–60.
30. Ying W, Riopel M, Bandyopadhyay G, Dong Y, Birmingham A, Seo JB, et al. Adipose tissue macrophage-derived exosomal miRNAs can modulate in vivo and in vitro insulin sensitivity. Cell. 2017;171:372-84.e12.
31. Quast C, Pruesse E, Yilmaz P, Gerken J, Schweer T, Yarza P, et al. The SILVA ribosomal RNA gene database project: improved data processing and web-based tools. Nucleic Acids Res. 2013;41:D590–6.
32. Callahan BJ, McMurdie PJ, Rosen MJ, Han AW, Johnson AJ, Holmes SP. DADA2: high-resolution sample inference from Illumina amplicon data. Nat Methods. 2016;13:581–3.
33. McMurdie PJ, Holmes S. phyloseq: an R package for reproducible interactive analysis and graphics of microbiome census data. PLoS ONE. 2013;8: e61217.
34. Aron-Wisnewsky J, Vigliotti C, Witjes J, Le P, Holleboom AG, Verheij J, et al. Gut microbiota and human NAFLD: disentangling microbial signatures from metabolic disorders. Nat Rev Gastroenterol Hepatol. 2020;17:279–97.
35. Miyauchi E, Shimokawa C, Steimle A, Desai MS, Ohno H. The impact of the gut microbiome on extra-intestinal autoimmune diseases. Nat Rev Immunol. 2023;23:9–23.
36. Behera J, Ison J, Tyagi SC, Tyagi N. The role of gut microbiota in bone homeostasis. Bone. 2020;135: 115317.
37. Liu S, Zhao W, Lan P, Mou X. The microbiome in inflammatory bowel diseases: from pathogenesis to therapy. Protein Cell. 2021;12:331–45.
38. Crost EH, Coletto E, Bell An, Juge N. *Ruminococcus gnavus*: friend or foe for human health. FEMS Microbiol Rev. 2023. https://doi.org/10.1093/femsre/fuad014.
39. Grahnemo L, Nethander M, Coward E, Gabrielsen ME, Sree S, Billod JM, et al. Cross-sectional associations between the gut microbe *Ruminococcus gnavus* and features of the metabolic syndrome. Lancet Diabetes Endocrinol. 2022;10:481–3.
40. Villa CR, Ward WE, Comelli EM. Gut microbiota-bone axis. Crit Rev Food Sci Nutr. 2017;57:1664–72.
41. Guan Z, Xuanqi Z, Zhu J, Yuan W, Jia J, Zhang C, et al. Estrogen deficiency induces bone loss through the gut microbiota. Pharmacol Res. 2023;196: 106930.
42. Guo Y, Jia X, Cui Y, Song Y, Wang S, Geng Y, et al. Sirt3-mediated mitophagy regulates AGEs-induced BMSCs senescence and senile osteoporosis. Redox Biol. 2021;41: 101915.
43. van de Vlekkert D, Demmers J, Nguyen X-X, Campos Y, Machado E, Annunziata I, Huimin H, Gomero E, Qiu X, Bongiovanni A, Feghali-Bostwick CA, D'Azzo A. Excessive exosome release is the pathogenic pathway linking a lysosomal deficiency to generalized fibrosis. Science Advan. 2019. https://doi.org/10.1126/sciadv.aav3270.
44. Chen CY, Rao SS, Ren L, Hu XK, Tan YJ, Hu Y, et al. Exosomal DMBT1 from human urine-derived stem cells facilitates diabetic wound repair by promoting angiogenesis. Theranostics. 2018;8:1607–23.
45. Luo ZW, Li FX, Liu YW, Rao SS, Yin H, Huang J, et al. Aptamer-functionalized exosomes from bone marrow stromal cells target bone to promote bone regeneration. Nanoscale. 2019;11:20884–92.
46. Wang ZX, Luo ZW, Li FX, Cao J, Rao SS, Liu YW, et al. Aged bone matrix-derived extracellular vesicles as a messenger for calcification paradox. Nat Commun. 2022;13:1453.
47. Cheng-Jang W, Cho S, Huang H-Y, Chun-Hao L, Russ J, Cruz LO, Franco F, da Cunha M-C, Chen LLL, Warner LM, Liao H-K, Utzschneider DT, Quon S, Berner J, Camara NOS, Zehn D, Belmonte JCI, Chen L-C, Huang S-F, Kuo ML, Li-Fan L. MiR-23~27~24–mediated control of humoral immunity reveals a TOX-driven regulatory circuit in follicular helper T cell differentiation. Sci Advan. 2019. https://doi.org/10.1126/sciadv.aaw1715.
48. Chandrasekaran AR, MacIsaac M, Dey P, Levchenko O, Zhou L, Andres M, Dey BK, Halvorsen K. Cellular microRNA detection with miRacles: microRNA- activated conditional looping of engineered switches. Sci Advan. 2019. https://doi.org/10.1126/sciadv.aau9443.
49. Zhang J, Huang Y, Shao H, Bi Q, Chen J, Ye Z. Grape seed procyanidin B2 inhibits adipogenesis of 3T3-L1 cells by targeting peroxisome proliferator-activated receptor gamma with miR-483-5p involved mechanism. Biomed Pharmacother. 2017;86:292–6.
50. Chen K, He H, Xie Y, Zhao L, Zhao S, Wan X, et al. miR-125a-3p and miR-483-5p promote adipogenesis via suppressing the RhoA/ROCK1/ERK1/2 pathway in multiple symmetric lipomatosis. Sci Rep. 2015;5:11909.
51. Xia ZY, Hu Y, Xie PL, Tang SY, Luo XH, Liao EY, et al. Runx2/miR-3960/miR-2861 positive feedback loop is responsible for osteogenic transdifferentiation of vascular smooth muscle cells. Biomed Res Int. 2015;2015: 624037.

52. Hu R, Liu W, Li H, Yang L, Chen C, Xia ZY, et al. A Runx2/miR-3960/miR-2861 regulatory feedback loop during mouse osteoblast differentiation. J Biol Chem. 2011;286:12328–39.
53. Grinberg IR, Yin G, Borovok I, Miller MEB, Yeoman CJ, Dassa B, et al. Functional phylotyping approach for assessing intraspecific diversity of *Ruminococcus albus* within the rumen microbiome. FEMS Microbiol Lett. 2015;362:1–10.
54. Bolte LA, Vila AV, Imhann F, Collij V, Gacesa R, Peters V, et al. Long-term dietary patterns are associated with pro-inflammatory and anti-inflammatory features of the gut microbiome. Gut. 2021;70:1287–98.
55. Xu Z, Xie Z, Sun J, Huang S, Chen Y, Li C, et al. Gut microbiome reveals specific dysbiosis in primary osteoporosis. Front Cell Infect Microbiol. 2020;10:160.
56. Ma S, Qin J, Hao Y, Fu L. Association of gut microbiota composition and function with an aged rat model of senile osteoporosis using 16S rRNA and metagenomic sequencing analysis. Aging (Albany NY). 2020;12:10795–808.
57. BinEssa HA, Zou M, Al-Enezi AF, Alomrani B, Al-Faham MSA, Al-Rijjal RA, et al. Functional analysis of 22 splice-site mutations in the PHEX, the causative gene in X-linked dominant hypophosphatemic rickets. Bone. 2019;125:186–93.
58. Deng L, Liu Y, Wu Q, Lai S, Yang Q, Mu Y, et al. Exosomes to exosome-functionalized scaffolds: a novel approach to stimulate bone regeneration. Stem Cell Res Ther. 2024;15:407.
59. Zhu Q, Tang Y, Zhou T, Yang L, Zhang G, Meng Y, et al. Exosomes derived from mesenchymal stromal cells promote bone regeneration by delivering miR-182-5p-inhibitor. Pharmacol Res. 2023;192: 106798.

Publisher's Note